ADVANCED FUNCTIONAL MATERIALS
www.afm-journal.de

Antibacterial Surface Coatings from Zinc Oxide Nanoparticles Embedded in Poly(*N*-isopropylacrylamide) Hydrogel Surface Layers

*Véronique B. Schwartz, Franck Thétiot, Sandra Ritz, Sabine Pütz, Lars Choritz, Alexandros Lappas, Renate Förch, Katharina Landfester, and Ulrich Jonas**

Despite multiple research approaches to prevent bacterial colonization on surfaces, device-associated infections are currently responsible for about 50% of nosocomial infections in Europe and significantly increase health care costs, which demands development of advanced antibacterial surface coatings. Here, novel antimicrobial composite materials incorporating zinc oxide nanoparticles (ZnO NP) into biocompatible poly(*N*-isopropylacrylamide) (PNIPAAm) hydrogel layers are prepared by mixing the PNIPAAm prepolymer with ZnO NP, followed by spin-coating and photocrosslinking. Scanning electron microscopy (SEM) characterization of the composite film morphology reveals a homogeneous distribution of the ZnO NP throughout the film for every applied NP/polymer ratio. The optical properties of the embedded NP are not affected by the matrix as confirmed by UV-vis spectroscopy. The nanocomposite films exhibit bactericidal behavior towards *Escherichia coli* (*E. coli*) for a ZnO concentration as low as ≈0.74 μg cm^{-2} (1.33 mmol cm^{-3}), which is determined by inductively coupled plasma optical emission spectrometry. In contrast, the coatings are found to be non-cytotoxic towards a mammalian cell line (NIH/3T3) at bactericidal loadings of ZnO over an extended period of seven days. The differential toxicity of the ZnO/hydrogel nanocomposite thin films between bacterial and cellular species qualifies them as promising candidates for novel biomedical device coatings.

1. Introduction

Bacterial contamination of medical implants continues to be a major issue in hospitals worldwide due to the diversity of germs and resistance mechanisms.[1] According to annual reports of the European Center for Disease Prevention and Control (ECDPC), the most frequent hospital-acquired infections, such as urinary tract, respiratory tract, and bloodstream infections, are commonly associated with implants. In vivo bacterial colonization of surfaces is a multistep-process of complex interactions between the pathogen, the host and the implant interface, resulting in a biofilm formation with much higher resistance to antibiotics compared to planktonic bacteria.[2] Amongst the common strains, *Escherichia coli* (*E. coli*) has shown a Europe-wide increase in resistance to all antibiotic classes tested.[3] Therefore, the ongoing research towards new antimicrobial coatings is of substantial relevance.

In this context, inorganic nanoparticles (NP) have shown great potential in the

Dr. V. B. Schwartz, Dr. S. Ritz, S. Pütz, Dr. R. Förch, Prof. K. Landfester
Max Planck Institute for Polymer Research
Ackermannweg 10, 55122 Mainz, Germany
Dr. F. Thétiot
UMR CNRS 6521
Université de Bretagne Occidentale
29285 Brest, France
Dr. F. Thétiot, Dr. A. Lappas
Foundation for Research and Technology–Hellas (FORTH)
Institute of Electronic Structure and Laser (IESL)
Nikolaou Plastira 100, Vassilika Vouton, 71110 Heraklion, Greece
Dr. L. Choritz
University Medical Center Mainz
BiomaTiCS research group
Department of Ophthalmology
Langenbeckstraße 1, 55131 Mainz, Germany
Prof. U. Jonas
Macromolecular Chemistry
Department Chemistry and Biology
University of Siegen
Adolf-Reichwein-Strasse 2, 57076 Siegen, Germany
E-mail:jonas@chemie.uni-siegen.de
Prof. U. Jonas
Foundation for Research and Technology–Hellas (FORTH)
Bio-Organic Materials Chemistry Laboratory (BOMCLab)
Nikolaou Plastira 100, Vassilika Vouton, 71110 Heraklion, Greece

DOI: 10.1002/adfm.201102980

biomedical sector due to their optical, catalytical and antimicrobial properties.[4] The most studied broad-spectrum antibiotic is silver,[5] which has a long history of antiseptic applications related to the treatment of burn wounds. Silver NP-impregnated products such as wound dressings, textile fabrics, and catheters have rapidly conquered the market.[6] However, there have been concerns about dose-related nanotoxicity towards healthy tissue[7] and the uncontrolled release of silver ions into the environment.[8] Yet, other inorganic NP have shown antibiotic properties such as gold,[9] copper,[10] CuO,[11] TiO_2,[12] and ZnO.[1b] ZnO NP are of particular interest due to their comparably modest cost and their established use in health care products.[13] Recently, several studies have demonstrated quite efficient antimicrobial activitiy of ZnO NP against gram-positive and gram-negative bacteria.[14] Several mechanisms of action have been proposed such as the formation of reactive oxygen species (ROS) or the release of Zn^{2+}-ions, both leading to harmful interactions with the bacterial cell membrane.[15] Most controversial reports can be found concerning their nanotoxicity towards healthy tissue.[14c,16] However, different sizes of the NP, capping agents, media, and assays employed, make it difficult to trace a general trend in the structure-property relations, thoroughly suggesting the necessity for a case-to-case study.

On the other hand, hydrogel surface coatings have been extensively used as support or protecting layer in food packaging[17] and tissue engineering.[18] Other important fields of hydrogels described in the literature are surface coatings for biocompatibilization; antifouling properties;[19] lubrication of implants, stents, and other medical devices; wound dressings; and controlled release in drug delivery.[20]

The combination of inorganic NP and hydrogel networks leads to the generation of new composite materials where the hydrogel matrix can benefit from the physical (mechanic, magnetic, optical, conducting, catalytic) and biomedical (antimicrobial, anticancer) properties of the embedded NP with unprecedented applications in biotechnology.[21]

Here, we present a novel composite material where ZnO NP are incorporated into a poly(N-isopropylacrylamide) (PNIPAAm) terpolymer matrix layer to generate a cost-effective system that is simple to use, stable, as well as biocompatible and that shows antibacterial properties against *E. coli*. The ZnO/hydrogel nanocomposites were prepared by simply mixing the PNIPAAm prepolymer with the ZnO NP suspension, followed by spin-coating and photocrosslinking similar to a previously reported procedure.[22] In addition to the full characterization of the separate components, scanning electron microscopy (SEM) was used to visualize the homogeneous distribution of ZnO NP within the hydrogel layer. Absorption measurements revealed that the optical properties of the ZnO NP were not affected by the incorporation into the hydrogel. However, depending on the NP loading, a material release into aqueous solution was observed with time. The fact that the embedded ZnO NP are considerably more efficient compared to reported ZnO NP concentrations in suspensions becomes apparent by the surface loadings, quantified by an inductively coupled plasma (ICP) emission spectrometer. Furthermore, the bactericidal amounts of embedded ZnO demonstrated a non-cytotoxic behavior towards mammalian cells (NIH/3T3), allowing for a healthy proliferation for 7 days as found in fluorimetric viability studies and flow cytometric measurements.

2. Results and Discussion

Many synthesis approaches of polymer-based nanocomposite materials rely on in situ generation of the nanomaterial inside of an appropriate matrix system such as the reduction of metal salts, ball milling, plasma polymerization in combination with metal deposition, and co-evaporation of a metal and an organic component.[23] However, they often suffer from relatively poor control over the particle characteristics and the distribution of the filler particles.[24] The advantages of the selected two-step procedure, i.e., the distinct synthesis of both components and subsequent incorporation of the nanocrystals into the hydrogel, first comprise an independent optimization of the synthesis conditions for the individual components (e.g., size and shape of the nanocrystals). Secondly, the two-step procedure allows for a detailed characterization of both components and, thirdly, the composites are easily prepared at low temperatures under mild conditions. In contrast to in situ precipitation methods, the polymer will not be contaminated by unconverted precursor material and/or by-products.[25]

2.1. Synthesis and Characterization of ZnO NP

Well-defined, single-crystalline ZnO NP were synthesized via high-temperature decomposition of zinc acetylacetonate in a binary surfactants medium of oleylamine and oleic acid. The high-temperature process induces the nucleation and permits a controlled growth of the resulting ZnO NP.[26] The transmission electron microscopy (TEM) image in **Figure 1**A shows the angular morphology of the ZnO NP in quite a homogeneous size distribution of the sample with an average particle size of 23 ± 6 nm as determined by complementary analysis from TEM and photon correlation spectroscopy (PCS) (Figure 1B). The size range of the ZnO NP was adjusted to match the minimum thickness of the ZnO/PNIPAAm nanocomposite thin films (60–80 nm in the dry state).

Figure 1D shows the X-ray powder diffraction pattern of the ZnO NP. The sharp peaks, indicating the crystalline character of the material, can be assigned to reflections from characteristic crystal planes of the ZnO Wurtzite structure (hexagonal phase, space group: $P6_3mc$, with lattice constants $a = b = 3.249$ Å, $c = 5.206$ Å, JCPDS, Card No. 36-1451). The crystallite sizes were calculated from the Scherrer equation based on the full width at half-maximum of designated peaks, which correspond to reflections from the 100, 002, and 110 crystal planes. The obtained values in the range of 12–17 nm are consistent with crystallite sizes of single NP measured by high-resolution TEM (HRTEM) (Figure 1C), suggesting the absence of any significant defects in the crystal structure. The single crystalline nature of the ZnO NP was ultimately confirmed by correlating the lattice fringes on the HRTEM image to the corresponding selected area electron diffraction pattern. The selection of adequate surfactants for the nanocrystals is

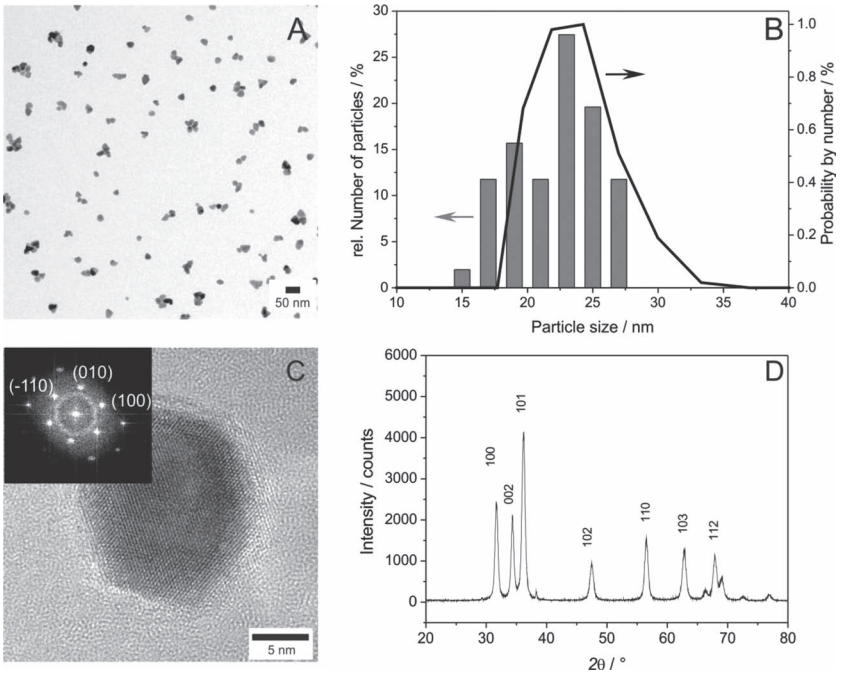

Figure 1. A) TEM image and B) corresponding size distribution by TEM (histogram) and PCS (black line) of the ZnO NP. C) HRTEM image displaying lattice-fringes of a distinct ZnO nanocrystal. Inset: selected area diffraction pattern confirming the crystalline ZnO phase. D) X-ray powder diffraction pattern of the ZnO NP.

critical in anticipation of their subsequent incorporation into the PNIPAAm hydrogel matrix. Because of their hydrophobic organic coating, the ZnO NP display a good dispersibility and stability with time in nonpolar solvents (e.g., chloroform), which are suitable for the dissolution of the PNIPAAm polymer.

2.2. Film Preparation and Characterization

2.2.1. Film Morphology

The ZnO/PNIPAAm nanocomposite films were prepared by mixing both components in different compositions of 1, 5, 10, 15, 25, and 35 wt% of ZnO in PNIPAAm into chloroform, evaporating the solvent, and redispersing the blend in ethanol. Spin-coating of these blends on silanized glass substrates (BP-silane, see Experimental Section) led to smooth films that were crosslinked by UV-irradiation. By using polymer contents of 2 or 5 wt%, different film thicknesses could be obtained, which will be further denoted as thin films (d = 60–85 nm) and thick films (d = 230–400 nm). SEM images of the composite film surfaces showed a homogeneous distribution of the ZnO NP at the surface of the thin films, for every NP/polymer ratio and even for very high NP loadings (**Figure 2**). A cross-sectional SEM image of a 382 nm thick film also revealed a good distribution of NP throughout the hydrogel matrix. The absence of pronounced agglomerates led us to conclude a partial stabilization of the ZnO NP within the hydrogel matrix by attractive interactions between the COOH groups of the polymer backbone and the NP surface, partially replacing surface-adsorbed oleic acid moieties. Indeed, ligand exchange between nanosized inorganic oxide surfaces and carboxyl or hydroxyl groups of natural organic compounds has been widely observed in aqueous environments.[27] Our assumption is supported by SEM studies of composite films, spin-coated from chloroform and ethanolic solutions (data shown in Figure S3, Supporting Information). The resulting thin films displayed a homogeneous NP distribution for both solvents although ethanol is a precipitating solvent for the native ZnO NPs. Additionally, when dispersed into the non-crosslinked polymer during the solution mixing process, the ZnO NP could be easily resuspended in ethanol. In short, these simple observations suggest that the NP are not influenced by the solvents used as a result of internal stabilization within the hydrogel matrix. Due to high viscosity of the sample solutions with increasing amounts of ZnO NP, the spin-coating procedure is limited to a production of thick composite films with a NP content of maximum 15 wt%.

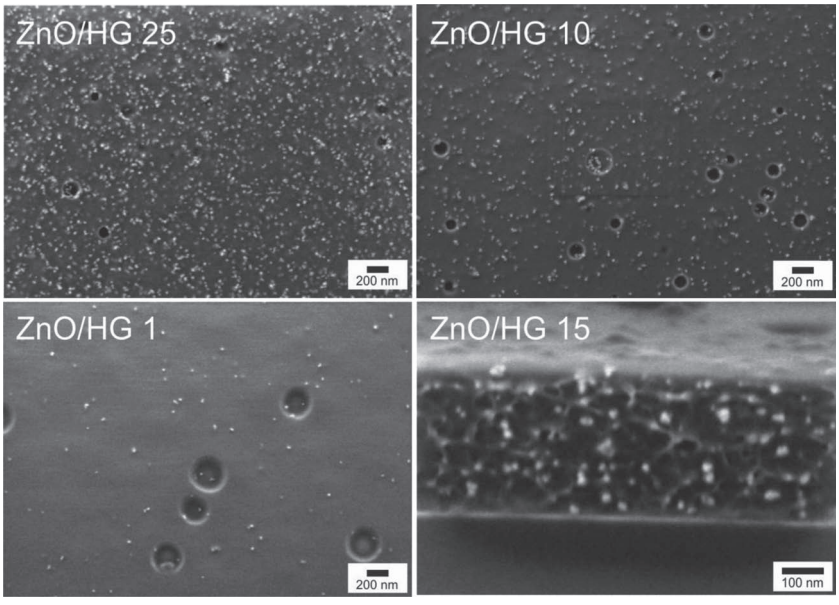

Figure 2. SEM images of ZnO/PNIPAAm nanocomposite thin films (d = 60–85 nm) with varying ZnO contents of 25, 10, and 1 wt% respectively. The circular holes are due to air bubbles in the spin-coating solutions. Cross-sectional image of a ZnO/PNIPAAm nanocomposite thick film (d = 382 ± 2 nm) with a ZnO content of 15 wt%.

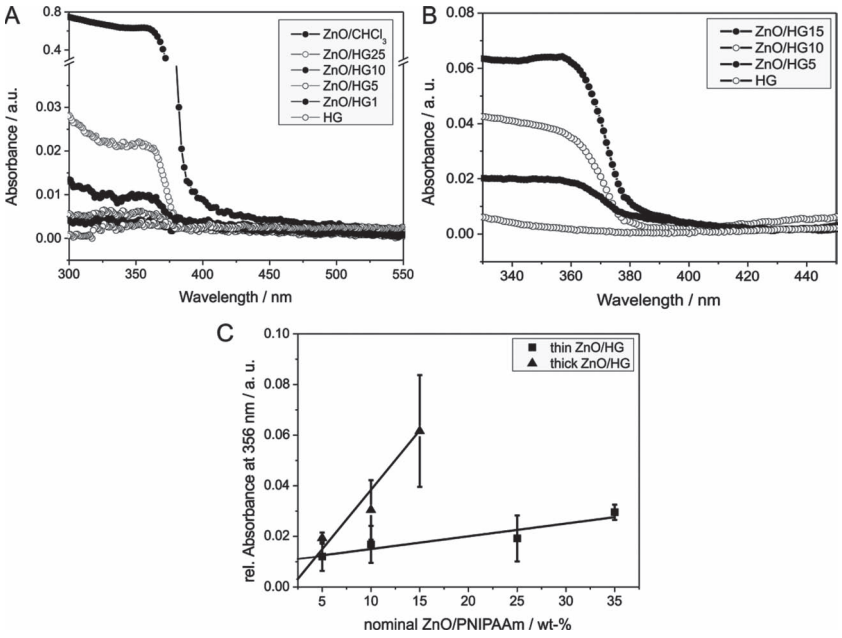

Figure 3. Absorption spectra of A) thin and B) thick ZnO/hydrogel (HG) nanocomposite films with varying ZnO NP content compared to free ZnO NP in chloroform. C) Absorbance at 356 nm of the different films plotted versus the NP content within the hydrogel layers.

2.2.2. Optical Properties of the Nanocomposite Films

Second to the morphology, the optical properties of the nanocomposite films were investigated. The photoluminescent properties of ZnO nanomaterials with a sharp excitation edge around 370–350 nm have been widely studied.[28] A change of their optical properties upon inclusion into the hydrogel could hint for significant chemical modifications of the ZnO material. To clarify this aspect, UV-vis absorption spectra of different ZnO/PNIPAAm nanocomposite films with varying NP content were recorded on quartz glass (**Figure 3**) and compared to the UV-absorbance of neat ZnO NP in chloroform. Inspection of Figure 3A reveals an absorption edge around 356 nm of the ZnO/PNIPAAm nanocomposite thin films in good agreement with the absorption signal of the free NP in chloroform with decreasing intensity related to the NP content. Similar results were obtained for thicker films (Figure 3B). As a proof-of-principle, the intensity of the excitation edge was plotted against the NP content (Figure 3C) for thin and thick composite films to verify the linear relation according to Beer–Lambert law. Though the relation holds true for the thick films, the linear extrapolation of the fitted thin film data does not cross the *x*-axis at zero wt% of ZnO. These results can be attributed to material losses at higher ZnO concentrations due to synergistic effects of centrifugal forces and the low viscosity of the thin film sample solutions. Nevertheless, the absorption spectra clearly indicate that the incorporation of the ZnO NP into the hydrogel matrix does not alter their optical properties, excluding any significant chemical modifications of the ZnO NP.

2.2.3. NP Loading within the Hydrogel Layers

The loading of zinc in the hydrogel matrix was measured by elemental analysis using an ICP optical emission spectrometer (OES). The resulting volume concentrations within the hydrogel were calculated by normalizing the measured amount of zinc with the total surface area of the coated glass slides multiplied with the film thickness in the dry state (**Figure 4**A). Conversely, the thickness of the dry thin films scales with other NP-polymer composite thin films documented in the literature, e.g., plasma-polymerized films and polyelectrolyte multilayers.[23a,29] Hence, the zinc amount was additionally expressed as loading per surface area (Figure 4B) to facilitate direct comparison with published data. Inspection of Figure 4A reveals a good correlation between the ZnO content used for the film preparation and the final zinc content measured by ICP. Second, it denotes similar volume concentrations in both thin and thick films of the same NP content, suggesting the volume concentration to be independent of the film thickness. This observation is quite interesting because it confirms the uniform distribution of the ZnO particles within the hydrogel matrix as already seen by SEM. Furthermore, it shows that the NP loading can be tuned by simple variation of the film thickness. The exact values per surface and volume fractions are summarized in Table 1 in the Supporting Information. The values obtained from 1 wt% ZnO/PNIPAAn films have not been listed because they were close to the detection limit of the ICP method. After conversion of measured values for zinc into ZnO, the amount of ZnO per surface area ranges from 0.35–2.17 μg cm^{-2} for thin (5–25 wt% ZnO) and 1.25–7.95 μg cm^{-2} for thick films (5–15 wt% ZnO). In comparison, the corresponding volume concentrations of 0.04–0.16 g cm^{-3} (0.58–2.5 mmol cm^{-3}) for the thin and 0.041–0.22 g cm^{-3} (0.63–3.36 mmol cm^{-3}) for the thick films appear

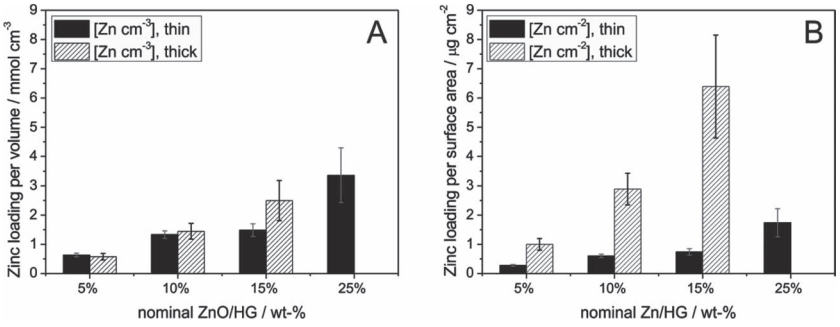

Figure 4. Zinc loading expressed as A) volume concentration (mmol cm^{-3}) of the hydrogel layer and B) amount per surface area (μg cm^{-2}) as determined by ICP-OES. Due to increased viscosity of the sample solutions, the spin-coating procedure is limited to a maximum ZnO content of 15 wt% for the thick nanocomposite films.

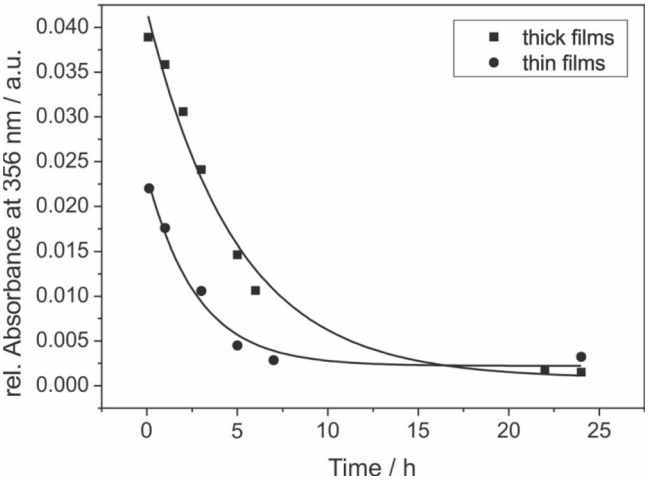

Figure 5. Absorbance at 356 nm of quartz glass coated with a thin (25 wt%) and thick ZnO/HG film (15 wt%) at different times while being rinsed for 24 h with buffer solution at room temperature.

very high. However, one has to consider the low dimensions of the film thickness in relation to the volume of 1 cm^3.

2.2.4. Release Experiments

In order to gain further insight into the dynamic behavior of the composite films in aqueous media, UV-vis experiments were performed on hydrated ZnO/PNIPAAm nanocomposite films. The absorbance at the absorption edge provides a convenient measure to monitor a potential ZnO NP release or degradation from the swollen hydrogel through time-dependent absorption measurements of coated quarz slides in phosphate buffered saline (PBS) buffer (0.01 M). Therefore, coated surfaces of 25 wt% thin and 15 wt% thick composite films were mounted into a teflon flow cell which was rinsed with buffer for 24 h at 0.1 mL min^{-1} at room temperature. Simultaneously, absorption spectra were recorded at various time spans up to 24 h. The results are displayed in **Figure 5**, which shows the absorbance of thin and thick nanocomposite films plotted against the measuring time. For 25 wt% thin film, a total loss of the ZnO absorption edge can be observed after 7 h of immersion in the buffer solution, suggesting a significant release or degradation of ZnO into the surrounding media. A slower decay of the absorption edge is found for a 15 wt% thick film. These results confirm our previous findings by ICP measurements that the NP loading is only dependent on the layer thickness of the hydrogel, which enables one to adjust it according to a desired application. The kinetic measurements do not afford any information about the nature of the released material, whether complete NP, some degraded species or zinc ions. However, it gives us a hint that the bactericidal mechanism is related to some interaction of the cells with the released species rather than surface-bound material. Furthermore, it is evident that the release time can be modulated by the thickness of the hydrogel layer. SEM analysis of the 25% thin film after 24 h of rinsing revealed the presence of few ZnO NPs at the surface (Figure S5, Supporting Information). Although the absorption signal decays to zero, the SEM image shows that the number of ZnO NP within the hydrogel film is reduced during the rinsing process but not completely zero. The amount of the remaining NP is apparently below the detection limit of the spectrometer. On the other hand, the size of the remaining NP is the same as the initial dimensions of the untreated particles, as seen by TEM. This implies that the NP are released from the hydrogel matrix as complete entity as opposed to a dissolution process, which would reduce the particle size, but not the number of particles.

2.3. Antimicrobial Activity of the ZnO/PNIPAAm Nanocomposite Films

To determine the antimicrobial activity of the ZnO/PNIPAAm nanocomposite films against *E. coli*, hydrogel layers of different thicknesses and varying amounts of ZnO were prepared on glass coverslips and exposed to a bacterial suspension for 24 h at 37 °C. Surviving cells were harvested from the surface and grown on agar plates for the assessment of colony forming units (CFU). Uncoated glass slides and pure hydrogel-coated slides served as control surfaces. The results are presented in **Figure 6**A as CFU relative to pure hydrogel surfaces of thin and thick films with increasing concentrations of ZnO NP (1–10 wt%). Furthermore, they are visualized by a photograph of the agar plates of undiluted and diluted material collected from a thin film samples series (Figure 6B). Inspection of Figure 6B allows several observations: First, the bacteria grow very well on both control surfaces, which can be readily observed by the bacterial lawn on the corresponding agar plates of the photograph. Second, there is a visible growth reduction throughout the sample series with increasing NP content. Taking into account the quantified results of Figure 6A, bacterial suspensions incubated on thin ZnO/PNIPAAm nanocomposite films were bactericidal starting from 10 wt% of ZnO relative to the polymer. Bacteriostatic behavior was still observed for NP contents as low as 1 wt% of ZnO. Most significantly, thicker nanocomposite films exhibited even higher levels of antimicrobial activity, as can be observed in an additional photograph in the Supporting Information (Figure S6). Whereas colonies easily formed on the pure hydrogel surfaces, a 100% reduction in CFU of *E. coli* occurred, starting from 5 wt% of ZnO. Based on these observations, the minimum inhibitory concentration (MIC) amounts to 10 wt% of ZnO for the thin and 5 wt% of ZnO for the thick films. According to the ICP measurements (Figure 4B), the zinc surface concentrations for the 10 wt% thin and 5 wt% thick films are in the same range. Thus, the MIC of ZnO per surface area spans from 0.74 to 1.25 μg cm^{-2}, which correspond to 4.7–7.8 μg mL^{-1} of ZnO in suspension. In contrast, most studies related to ZnO NP investigated their antibacterial effect in suspension with a MIC in the range of 1–35 mM (81–2835 μg mL^{-1}), depending on the NP size, the bacterial strain and the applied assay.[30] To the best of our knowledge, only few studies focused on ZnO NP on composite surfaces.[31] Comparable antimicrobial efficiencies against *S. epidermidis* have been reported by Agarwal et al. with 0.4 μg cm^{-2} of silver NP embedded in polyelectrolyte multilayers.[23a] Therefore, we strongly recommend the exploration of ZnO NP as an efficient alternative to nanoparticulate silver systems.

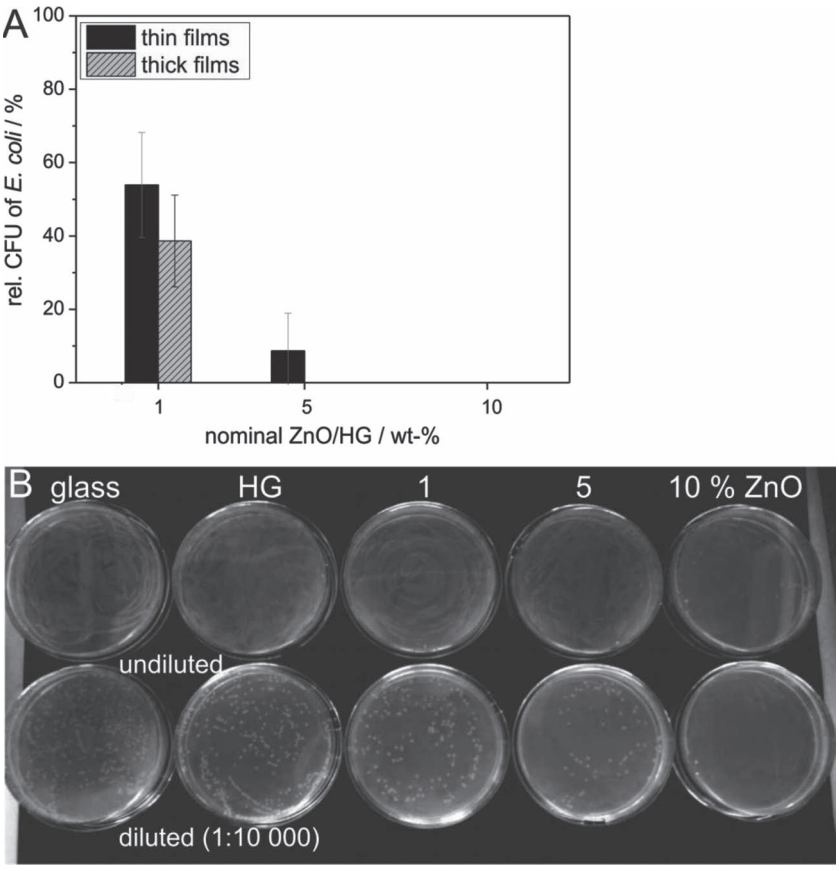

Figure 6. A) The effect of thin or thick hydrogels with increasing concentrations of ZnO NP (1–10 wt%) on the growth of *E.coli*, expressed as CFU relative to the pure hydrogel (HG). Mean values and standard deviation have been calculated from three independent experiments. B) Photograph of *E.coli* colonies grown on agar plates after exposure to different thin ZnO/HG nanocomposite films.

Previous reports in the literature have shown that smaller NP with increasing surface to volume ratios resulted in stronger antimicrobial effects against various bacteria under ambient light conditions,[30,32] whereas the ZnO NP shape and crystalline structure seemed to have less effect.[33] Hence, we suppose that the antibacterial effect of our ZnO/hydrogel nanocomposite films are determined by the small NP size (≈20 nm), the uniform distribution of the filler particles within the hydrogel and the controlled release in aqueous media.

Several, probably accumulative, mechanisms such as direct disruptive electrostatic interactions of NP with cell walls and membranes[15a,34] or indirect effects due to the decomposition of ZnO and the formation of reactive oxygen species (H_2O_2, hydroxyl radicals (•OH), singlet oxygen ($^1O_2$))[31c,32b,33b,35] or Zn^{2+}[15b] have been discussed. Besides, the medium is known to influence the toxicity of ZnO NP due to complexation of zinc ions and precipitation of zinc salts. Amplified antibacterial activities were further observed by photocatalytical UV or light activation of ZnO NP.[30b,31b] Interestingly, all our experiments have been conducted in the absence of light, which excludes any photoactivation processes. However, our current studies provide little information on the mechanism of action. Nevertheless, the UV kinetic in aqueous medium has demonstrated a time-dependent ZnO NP reduction, suggesting a diffusional mechanism of interaction between the nanomaterial and the bacterium rather than contact-active interactions with surface-bound NP.

2.4. Cytotoxicity of the PNIPAAm/ZnO Nanocomposite Films

2.4.1. Cell Viablility

Parallel to the antibacterial activity, we sought to determine the interactions of mammalian cells with our ZnO/hydrogel nanocomposite films. The attachment and spreading of NIH/3T3 Swiss mouse fibroblasts was investigated by a fluorimetric viability/proliferation test as well as by flow cytometry (fluorescence activated cell sorting, FACS). For the flow cytometric analysis, the cells were cultivated on nanocomposite-coated surfaces and the viability was detected after 24 h, using Annexin V coupled to fluoresceinisothiocyanate (FITC) and propidium iodide (PI) staining to differentiate between viable, apoptotic, and necrotic cells. Uncoated, hydrogel-coated (PNIPAAm) as well as surfaces coated with a commercially available hydrogel-based ultralow attachment surface (ULA) served as control. The results are summarized in **Figure 7**. Inspection of Figure 7 reveals that the number of vital cells decreased after

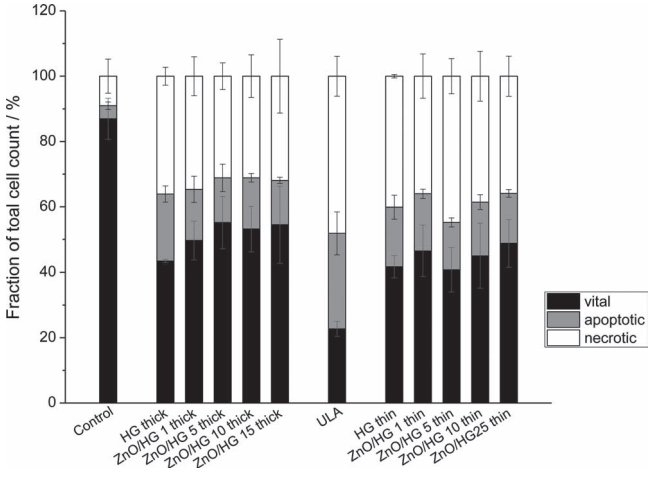

Figure 7. Viability of NIH/3T3 Swiss mouse fibroblasts after 24 h exposure to different ZnO/hydrogel nanocomposite thin and thick films (5–25 wt% of ZnO) as determined by flow cytometry. The ULA surface is a commercially available hydrogel-coated cell culture dish/well plate, designed for non-adherent cell cultures.

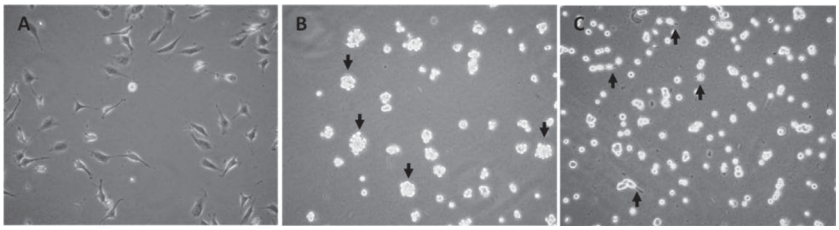

Figure 8. NIH/3T3 Swiss mouse fibroblasts after 24 h of incubation on different surfaces. A) Uncoated control surface, B) PNIPAAm-coated surface with downward arrows pointing out aggregates of 20–30 cells, and C) ZnO/PNIPAAm nanocomposite thick film (15 wt% of ZnO). Upward arrows show attached cells with small cellular protrusions.

exposure to different NP-free hydrogel formulations (40.8–55.5% in PNIPAAm, 22.7% in ULA) compared to uncoated control surfaces (87.0 ± 8.9%). Consequently, the rate of apoptosis (13.6–20.4% in PNIPAAm, 29.2% in ULA vs. 4.0% in Control) and necrosis (29.8–44.8% in PNIPAAm, 48.1% in ULA vs. 9.1% in control) increased. Two-way analysis of variance (ANOVA) revealed that this highly significant effect was largely due to the presence of the hydrogels (Wilks–Lambda = 0.287, $p < 0.001$), while ZnO NP did not contribute to the decrease in cell viability (Wilks–Lambda = 0.793, $p = 0.909$). Tukey-corrected post hoc comparisons could not detect any significant differences between the different ZnO NP concentrations.

The in vitro cytotoxicity assays demonstrated that the ZnO/PNIPAAm nanocomposites were not generally toxic to NIH/3T3 Swiss mouse fibroblasts seeded onto the coatings for 24 h. The apparently high number of lost cells on all pure hydrogel and ZnO-doped surfaces were most likely not the result of direct hydrogel toxicity but rather stem from the cells' inability to attach to the hydrogel surface. Like most tissue-bound cells, fibroblasts are anchorage-dependent. Therefore, fibroblasts are more resistant to continued suspension than other cell types (e.g. epithelial cells), and will reversibly arrest their cell cycle, until they can attach to a surface. However, they too will eventually undergo apoptosis if kept in suspension for an extended period of time[36]. **Figure 8** outlines the cell morphology on uncoated control surfaces (Figure 8A), PNIPAAm-coated (Figure 8B), and a ZnO/PNIPAAm coated thick film (15 wt%) (Figure 8C) after 24 h of incubation. Whereas the cells on the uncoated control surface attached and spread out normally, the fibroblasts on the pure PNIPAAm film clustered into large clumps (marked by downward arrows in Figure 8B). In contrast, the ZnO-doped thick film appeared to promote a slight attachment as can be seen by the formation of small cellular protrusions. The aggregation of cells exposed to PNIPAAm in our experiments may indicate the cells' attempts to adhere to their immediate environment. However, this does not fully prevent the onset of apoptosis, as shown by our flow cytometric assessment of cell viability.

The high rate of necrosis seen in our experiments is most likely a secondary effect due to the in vitro setup. In vivo, apoptotic cells are cleared away by macrophages, which were not present in our fibroblast monoculture. A large portion of apoptotic cells are likely to have ruptured during sample preparation for FACS analysis, which involved extended exposure to trypsin and some mechanical stress in the attempt to separate cell aggregates into single cells. This secondary rupture of the cell membrane allows for the uptake of propidium iodide into the fragmented nucleus of the cell, thus rendering it difficult to distinguish from a primarily necrotic cell.

Previous studies of crosslinked PNIPAAm have shown antifouling properties both to proteins and primary human fibroblasts.[18c,20b,37] We therefore used a commercially available type of hydrogel-coated culture dish as a positive control in order to evaluate any effects of the expected inhibition of cell attachment on PNIPAAm-coated surfaces. Our positive control surface (ULA) is commonly used for suspension cultures of non-adherent cell types (e.g., leukocytes, hematopoietic stem cells) without any reported detrimental effects. Interestingly, the rate of apoptosis and (secondary) necrosis was highest in the cells seeded onto the ULA surface. Thus, it appears reasonable to conclude from our experiments, that the photocrosslinked PNIPAAm used in this study is not in itself toxic to NIH/3T3 fibroblasts.

It was interesting to note that with increasing concentration of the ZnO NP embedded in the hydrogel, the number of cells that are able to adhere to the hydrogel also increased (up to approximately 10% of all cells, Figure 8C). The cell attachment might be a result of differences in the surface topography of the hydrogels with ZnO particles protruding from the surface, potentially enabling cell adherence. An alternative explanation might be changes in the degree of crosslinking of the terpolymer due to the UV-absorption of the ZnO-NP, thus locally altering the non-fouling properties of the hydrogel. Although not very pronounced, this increase in cell attachment could result in an increase of cell viability that could potentially mask a minor toxic effect of ZnO NP. However, as of now, this remains speculative.

2.4.2. Cell Proliferation

Due to the lack of attachment of the fibroblasts, the cells were reseeded after 24 h of exposure to various ZnO/hydrogel nanocomposite films. Cell proliferation was indirectly tracked by repeated fluorometric measurements over a period of 7 days of metabolically reduced resofurin in the culture medium. As illustrated in **Figure 9**A, the proliferation was unaltered by the exposure to hydrogel thin films compared to the control surface, with increasing ZnO concentrations not affecting the rate of proliferation. In contrast to the apparent absence of an immediately toxic effect seen in the FACS-analysis, long-term observation of the cells showed, that ZnO may have some influence on cell function (Figure 9B). Exposure to concentrations higher than 10 wt% of ZnO embedded in the thick hydrogel films, led to a moderate slowing of cell proliferation. While this effect did not reach statistical significance in our experimental series due to a large variability between the separate experiments (Repeated Measures ANOVA, Greenhouse-Geisser-corrected $p = 0.155$), it is well in accordance with recent reports on the cytotoxicity of ZnO NP towards mammalian cells.[38] These studies indicate a preferential toxicity of ZnO NP to rapidly proliferating cells (i.e., cancerous cells or stem cells), while slowly or non-proliferating cells can tolerate higher concentrations

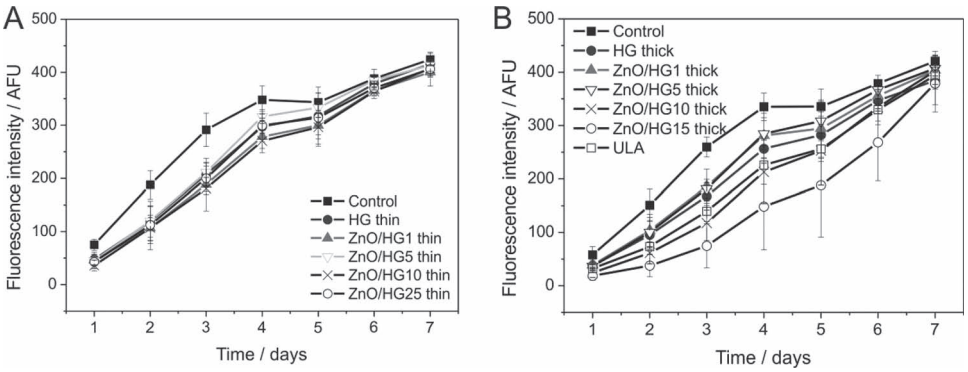

Figure 9. Proliferation of NIH/3T3 Swiss mouse fibroblasts after 24 h exposure to different a) thick and b) thin ZnO/hydrogel (HG) nanocomposite films with varying ZnO NP contents (1–25 wt%).

of ZnO. Taccola et al.[38c] suggested that this difference is caused by the more rapid ZnO-dependent production of reactive oxygen species. More interestingly, this differential effect may also provide an explanation for the apparent discrepancy between our own viability and proliferation results. As mentioned before, fibroblasts in suspension (as caused by seeding onto our PNIPAAm hydrogel) will change into the quiescent state of the cell cycle (G0-Phase) and thus not proliferate,[36,39] until they can attach. If ZnO NP are more toxic to proliferating cells, their lack of effect on cell viability in our experiments may be a direct result of the cells' inability to adhere.

In more practical terms, the relatively higher tolerance of non-proliferating cells to ZnO NP may be useful in clinical settings. An antiadhesive, bactericidal coating will most likely be employed on so-called "indwelling devices" such as respiratory tubing, urinary catheters, or intravenous catheters. In fact, more than two-thirds of all hospital-acquired infections are associated with the prolonged use of these three types of device.[40] Nanocomposite films with carefully tuned amounts of ZnO, coated onto such devices would typically come in contact with respiratory epithelium, urothelial cells, or vascular endothelium. Most of these cells are well differentiated and do not proliferate.

3. Conclusions

In this work, we have demonstrated a simple and cost-effective way to produce novel composite materials based on ZnO NP embedded in a biocompatible PNIPAAm hydrogel matrix. Surface and cross-sectional investigations of the composite material showed quite a uniform distribution of the filler particles within the hydrogel matrix with tunable loadings by simply varying the thickness of the thin film. Based on these results, a partial stabilization of the NP by ligand exchange between oleic acid and acrylic acid residues in the polymer backbone was postulated. The optical properties of the ZnO NP did not change through incorporation into the hydrogel layers. However, depending on the NP loading, a decay of the absorption signal could be observed with time upon immersion into aqueous solution, suggesting a NP release from the hydrogel matrix. The composite films exhibited efficient antimicrobial activity against *E. coli* at very low ZnO loadings of 0.74 μg cm^{-2} (1.33 mmol cm^{-3}) with bacteriostatic activity for as little as 0.1 μg cm^{-2} (0.04 mmol cm^{-3}). This contrasts to current studies with much higher ZnO NP concentrations for a comparable performance. However, similar antimicrobial activities have been reported for nanoscopic silver/polymer composites. Based on these findings, we strongly recommend the exploration of ZnO NP as an alternative to nanoparticulate silver systems. In completion to the antibacterial assay, viability studies with mammalian cells (NIH/3T3) demonstrated non-cytotoxic behavior of the nanocomposite films at bactericidal loading levels, permitting healthy proliferation for a period of 7 days. Interestingly, the ZnO-doped surfaces were found to slightly improve cell adhesion compared to pure hydrogel films. In conclusion, we have successfully demonstrated a new approach towards engineered surface coatings with large potential to reduce microbial contamination of biomedical devices.

4. Experimental Section

Materials: Zinc acetylacetonate monohydrate ($Zn(acac)_2{\cdot}H_2O$), oleic acid (OLAC, 90%), and oleylamine (OLAM, 70%), were purchased from Aldrich and used without further purification. All solvents used were of analytical grade and purchased from Aldrich and Riedel. Unless otherwise stated, all ZnO NP syntheses were carried out under anaerobic-inert conditions using a standard Schlenk technique while the extraction/purification procedures of the NP were carried out under ambient atmospheric conditions. The PBS was prepared by dissolving preformed tabs (0.01 M, pH = 7.4), which were purchased from Aldrich, into ultrapure water. Ultrapure water was obtained from a Milli-Q 185 Plus water purification system (Millipore). Lysogeny broth (LB) media with ampicillin (Amp) was prepared by dissolving bacteriological peptone (1% w/v, Fluka), yeast extract (0.5% w/v, Roth), and NaCl (1% w/v) in ultrapure water, adjusting the pH with 1 N NaOH to 7.0 and autoclaving the media for 20 min at 121 °C. The ampicillin (10 mg mL^{-1} sterile solution, Fluka) was added to the medium at room temperature to a final concentration of 10 mg mL^{-1}. For LB agar plates, 1.5% w/v agar (Fluka) was dissolved in LB media before autoclaving. Minimal LB media was used as a 10-fold dilution of the LB-media supplemented with 10 μg mL^{-1} ampicillin. The LB media and agar plates were stored at 4 °C and used within 30 days.

Synthesis and Characterization of ZnO Nanoparticles (NP): As a general procedure, ZnO NP were synthesized using zinc acetylacetonate monohydrate (5 mmol) as metal precursor in the presence of two distinct surfactants, namely oleylamine (15 mmol) and oleic acid (3 mmol). The

resulting mixture was initially submitted to a degassing process, and then heated under argon flux. The synthesis was carried out at 240 °C for 20 min under argon flow, to allow for the growth of the ZnO NP. After cooling, the resulting nanocrystalline product was extracted from the reaction mixture by precipitation upon addition of absolute ethanol. The product was separated by centrifugation and thoroughly purified by repeated cycles of dispersion in chloroform and reprecipitation with absolute ethanol to remove precursor and surfactant residuals. The final NP displayed a good dispersibility and shelf-life in chloroform due to their hydrophobic organic coating. After air drying, a white powder was obtained for X-ray diffraction and UV-vis absorption measurements. The ZnO NP concentration was determined by measuring the mass content upon solvent evaporation.

The morphology of the NP was characterized by TEM using a JEM 120 CX microscope working at an accelerating voltage of 100 kV. The samples were prepared by casting highly diluted NP dispersions from chloroform onto carbon-coated grids. HRTEM images were recorded with a Tecnai G2 F20 S-Twin with an accelerating voltage of 200 kV, equipped with a *Cs* corrector and automatic fine-tuning of astigmatism. X-ray diffraction studies were obtained from a Philips PW1820 X-ray powder diffractometer with Cu-K radiation. The crystallite size was calculated according to the Scherrer's equation[43]

$$D = \frac{0.9\lambda}{\beta\cos\theta}$$

where λ is the wavelength of the X-ray source, β the full width at half-maximum (FWHM) in radians, taken from the X-ray diffraction patterns, and θ the Bragg's diffraction angle. A NICOMP zetasizer, measuring at a fixed scattering angle of 90° was utilized to determine the particle size distributions by photon correlation spectroscopy. The measurements were carried out at 23 °C on diluted dispersions in chloroform.

Synthesis of the Terpolymer (PNIPAAm) The PNIPAAm terpolymer consisting of NIPAAm, methacrylic acid (MAA), and 4-benzophenone methacrylate (MABP) in a molar ratio of 90:5:1 was obtained by free radical polymerization as described in previous work.[41] ^{1}H NMR (250 MHz, methanol-d_4, δ): 1.03-1.30 (m,–CH_3), 1.30-1.84 (m,–CH_2–), 1.84-2.40 (m, NIPAAm backbone CH), 3.97 (s, CH_3–CH–CH_3), 7.10-8.20 (m, C–H_{arom}). Molecular weight (g mol^{-1}): M_w = 151 005, M_n = 65 154, PDI = 2.32 (gel permeation chromatography (GPC), dimethylformamide (DMF), poly(methyl methacrylate) (PMMA) standard).

Synthesis of 4-(3-Triethoxysilyl)propoxybenzophenone (BP-silane): 4-Allyloxybenzophenone was obtained by alkylation of 4-hydroxybenzophenone with allyl bromide as described in previous work.[41] The product (9.9 g, 50 mmol) was dissolved in triethoxysilane (4.8 mL, 550 mmol) at room temperature under argon flow. After the addition of the catalyst, (Pt on activated charcoal) the solution was stirred at room temperature until full conversion was proved by thin layer chromatography (TLC) (heptane: acetone 5:1.5: 4-allyloxybenzophenone retardation factor R_f = 0.48; BP-silane: R_f = 0.22) after 2 d. After filtering off the catalyst, the excess of triethoxysilane was removed in high vacuum and the yellowish product oil was stored in an ethanolic solution under argon and used without further purification. FD-MS (Field Desorption Mass Spectrometry): *m/z* (%): 402 (100) [M+], 805 (40) [2M+], 1207 (13) [3M+]. ^{1}H NMR (250 MHz, $CDCl_3$, δ): 0.77 (t, 2H, 3-propoxy), 1.23 (t, 9H, CH_3 ethoxy), 1.93 (td, 2H, 2-propoxy), 3.85 (q, 6H, CH_2 ethoxy), 4.02 (t, 2H, 1-propoxy), 6.95 (d, 2H, 3,5-phenone), 7.47 (t, 2H, 3,5-benzyl), 7.56 (t, 1H, 4-benzyl), 7.72 (d, 2H, 2,6-benzyl), 7.79 (d, 2H, 2,6-phenone).

Silanization of Glass Substrates: Glass coverslips (Thermo Scientific, Menzel Gläser) or quartz glass (PGO) were cut into 2.5 × 2.5 cm^2 pieces or 1.2 × 2.4 cm^2 pieces, respectively, cleaned by immersion and sonication in Hellmanex solution (Hellma optic), followed by repeated rinsing with ultrapure water and ethanol. The substrates were treated with a 5 mg mL^{-1} ethanolic solution of 4-(3-triethoxysilyl) propoxybenzophenone (BP-silane) for 24 h, dried for 1 h at 50 °C, thoroughly rinsed with ethanol and stored in dark containers under argon before use.

Preparation of the ZnO/PNIPAAm Nanocomposite Films: ZnO/PNIPAAm nanocomposite films were prepared by mixing both components in 2 or 5 wt% solutions of PNIPAAm in chloroform with varying NP/polymer ratios of 1, 5, 10, 15, 25, and 35 wt% ZnO. The chloroform was evaporated at room temperature and the components were redispersed in the equivalent amount of ethanol and homogenized by sonication and orbital shaking at 600 rpm. The sample solutions were spin-coated on silanized glass coverslips (2.5 × 2.5 cm^2), dried at 40 °C for 3 h and crosslinked by UV irradiation (365 nm) in a Stratalinker 2400 (Stratagene) for 60 min, which corresponds to a total photocrosslinking energy dose of 6.28 J cm^{-2}. All samples were stored in dark containers before further use.

Characterization of the ZnO/PNIPAAm Nanocomposite Films: Morphological characterization was performed using a Zeiss 1530 Gemini field emission scanning electron microscope (700 V at 2 mm WD; InLens detector). The samples were prepared by spin-coating the sample solutions on plasma-activated (partial pressure ratio of Ar to O2 *p*(Ar:O_2): 0.9:0.1 mbar, 300 W, 10 min) Si-wafer with subsequent drying and crosslinking. Energy-dispersive X-ray spectroscopy (EDS) was performed on selected samples at 2.5 kV using a Hitachi SU8000 coupled with a Bruker XFlash 5010. The film thickness was determined by a surface profiler (Tencor P10, alpha-stepper). For this purpose, composite films, spin-coated on plasma-activated Si-wafers, were scratched with a needle and subsequently scanned by the profiler to probe the depth of the film.

UV-vis absorbance spectra were recorded on a Lambda 900 spectrometer (Perkin Elmer), using coated quartz substrates. For the kinetic measurements in buffer solution (PBS, 0.01 M), a teflon flow cell (diameter = 5 mm, volume = 1 mL) with two quartz (PGO (Präzisions Glas @ Optik GmbH)) windows was employed, one of them coated with ZnO/PNIPAAm nanocomposite films of varying NP content. A peristaltic pump (Ismatec, Reglo Digital) controlled the flow while the sample cell was rinsed for 24 h at 0.1 mL min^{-1}. The concentration of Zn^{2+}-ions within the hydrogel layers was measured by elemental analysis with an ICP emission spectrometer (Horiba Jobin Yvon, Bernsheim, Germany) at λ = 328.233, 334.502, and 481.053 nm. To this end, different sample series of thin and thick films were prepared on glass substrates with varying amounts of ZnO NP. Zinc ions were extracted from the hydrogel matrix by immersing the coated slides into 65% nitric acid for 1 h. Aliquots of 0.5 mL were diluted to 5% nitric acid content and purified through filtration prior to ICP measurements (Millipore Millex-LS, hydrophobic PTFE 0.5 µm). The loading of zinc within the hydrogel film was calculated by normalizing the measured amount of zinc with the total surface area of the coated glass slides multiplied with the film thickness in the dry state.

Statistics: The mean value and standard deviation (SD) were calculated from at least three independent experiments for thickness, UV-vis, and ICP measurements.

Antimicrobial Activity To determine the antimicrobial activity of the ZnO/PNIPAAm nanocomposite films, coated glass coverslips were covered with a poly(dimethyl)siloxane mask, providing a defined area of 1 cm^2. The composite films were incubated with 300 µL of *E.coli* (TOP 10 with ampicillin resistance, Invitrogen) suspension, which is equivalent to ≈5 × 10^5 CFU mL^{-1}, in minimal LB media at 37 °C in a humidified chamber that prevented drying of the surfaces. After 24 h, the bacterial suspensions were collected and the composite films were washed three times with 150 µL minimal LB media. Bacteria suspensions and washing solutions were combined and 20 µL aliquots of serial dilutions (1:5000 or 1:10 000) in 1 mL minimal LB media were plated on LB agar plates for the determination of viable bacteria. The agar plates were incubated for another 24 h at 37 °C to give an estimate of viable cell counts as CFU. Uncoated glass slides and pure hydrogel slides served as control surfaces. The mean value and standard deviation (SD) was calculated from three independent experiments and the results expressed as CFU (%) relative to the pure hydrogel.

In Vitro Cytotoxicity Assay: Toxicity of the ZnO/hydrogel nanocomposite films to NIH/3T3 Swiss mouse fibroblasts (ATCC/LGC-Standards) was assessed by a fluorimetric viability/proliferation test as well as by determining the fraction of apoptotic and necrotic cells after 24 h exposure to hydrogel layers, doped with different concentrations of

ZnO nanoparticles. To this end, 2×10^6 cells were seeded into 60 mm standard culture dishes, coated with ZnO/HG nanocomposite films and incubated for 24 h at 37 °C and 5% CO_2 in air. As the majority of the cells did not attach to the coatings, direct morphological assessment of the cells could not be performed. For the viability assay, cells were therefore reseeded into non-coated 24-well plates (2×10^4 cells per well) and allowed to attach for 24 h. Culture medium was then replaced by a medium containing 10% (v/v) resazurin (PromoKine, Heidelberg), a nontoxic dye that freely diffuses through the cell membrane and is reduced to the highly fluorescent resofurin by metabolically active cells. After 4 h of incubation, the fluorescence of the supernatant medium was measured at excitation/emission wavelengths of 544/590 nm. This procedure was repeated every 24 h for 7 d, thus allowing for indirect measurement of cell proliferation since the emission intensity of resofurin is directly proportional to the number of viable cells.

For the detection of apoptosis/necrosis after 24 h exposure of the cells to the ZnO/HG nanocomposite films, cells were dually stained with Annexin V-FITC (AnV) and propidium iodide (PI) and analyzed by flow cytometry (FACSCalibur, BD Heidelberg, CellQuestPro software). AnV specifically binds to phosphatidyl serine, which is specifically located on the inner layer of the cell membrane of viable cells. In early apoptosis, membrane asymmetry is lost, exposing phosphatidyl serine to the outside of the cell within the reach of AnV. When the cell membrane ruptures in necrotic cells, both AnV and PI, which are normally excluded, are able to enter the cell. PI then intercalates into the nuclear DNA. Thus, the staining pattern is able to differentiate viable cells (AnV-/PI-) from apoptotic (AnV+/PI-) and necrotic cells (AnV+/PI+). Uncoated surfaces served as negative control; hydrogel-coated as well as surfaces coated with a commercially available ULA surface (Corning) served as positive control. All experiments were run in technical duplicates or triplicates and repeated on at least three separate occasions. Unless indicated otherwise, results were expressed as mean ± standard error of the mean. Statistical analysis was performed using SPSS (v18). For the proliferation assay, Greenhouse-Geisser-corrected repeated measures ANOVA was employed according to Ludbrook.[42] For analysis of flow cytometry results, two-way ANOVA was performed. The separate hydrogels and ZnO concentrations were compared in a Tukey-corrected post-hoc analysis. Statistical significance was assumed at $p < 0.05$.

Supporting Information

Supporting Information is available from the Wiley Online Library or from the author.

Acknowledgements

The authors would like to thank Michael Steiert for technical assistance with the ICP-OES and Gunnar Glasser for measuring SEM. Robert F. Roskamp is acknowledged for help with the synthesis of the PNIPAAm terpolymer, Patrick Duhr for assistance with the thickness measurements, and Ingo Lieberwirth for fruitful discussions concerning XRD and HRTEM. This project was funded by the European Union (FP7-Embek1, grant 211436) and by the Marie Curie Transfer of Knowledge program NANOTAIL (grant MTKD-CT-2006-042459).

Received: December 9, 2011
Published online: March 15, 2012

[1] a) K. Page, M. Wilson, I. P. Parkin, *J. Mater. Chem.* **2009**, *19*, 3819; b) I. Banerjee, R. C. Pangule, R. S. Kane, *Adv. Mater.* **2011**, *23*, 690; c) E. M. Hetrick, H. Schoenfisch, *Chem. Soc. Rev.* **2006**, *35*, 780; d) R. O. Darouiche, *Int. J. Artif. Organs* **2007**, *30*, 820.

[2] a) D. Davies, *Nat. Rev. Drug Discovery* **2003**, *2*, 114; b) L. Hall-Stoodley, J. W. Costerton, P. Stoodley, *Nat. Rev. Microbiol.* **2004**, *2*, 95.

[3] *European Centre for Disease Prevention and Control. Annual epidemiological report on communicable diseases in Europe 2010.* ECDC, Stockholm **2010**.

[4] a) A. Quarta, R. Di Corato, L. Manna, S. Argentiere, R. Cingolani, G. Barbarella, T. Pellegrino, *J. Am. Chem. Soc.* **2008**, *130*, 10545; b) H. R. Jafry, M. V. Liga, L. Qilin, A. R. Barron, *Environ. Sci. Technol.* **2010**, *45*, 1563; c) R. Prucek, J. Tucek, M. Kilianová, A. Panácek, L. Kvítek, J. Filip, M. Kolár, K. Tománková, R. Zboril, *Biomaterials* **2011**, *32*, 4704.

[5] D. R. Monteiro, L. F. Gorup, A. S. Takamiya, A. C. Ruvollo-Filho, E. R. d. Camargo, D. B. Barbosa, *Int. J. Antimicrob. Agents* **2009**, *34*, 103.

[6] a) D. Roe, B. Karandikar, N. Bonn-Savage, B. Gibbins, J. B. Roullet, *J. Antimicrob. Chemother.* **2008**, *61*, 869; b) M. Rai, A. Yadav, A. Gade, *Biotechnol. Adv.* **2009**, *27*, 76.

[7] P. V. AshaRani, G. Low Kah Mun, M. P. Hande, S. Valiyaveettil, *ACS Nano* **2008**, *3*, 279.

[8] L. Geranio, M. Heuberger, B. Nowack, *Environ. Sci. Technol.* **2009**, *43*, 8113.

[9] V. A. Nadtochenko, M. A. Radtsig, I. A. Khmel, *Nanotechnol. Russ.* **2010**, *5*, 227.

[10] N. C. Cady, J. L. Behnke, A. D. Strickland, *Adv. Funct. Mater.* **2011**, *21*, 2506.

[11] a) W. Zhang, Y. Zhang, J. Ji, Q. Yan, A. Huang, P. K. Chu, *J. Biomed. Mater. Res. A* **2007**, 838; b) O. Akhavan, E. Ghaderi, *Surf. Coat. Technol.* **2010**, *205*, 219.

[12] a) H. Kong, J. Song, J. Jang, *Environ. Sci. Technol.* **2010**, *44*, 5672; b) D. Mihailovic, Z. Saponjic, M. Radoicic, T. Radetic, P. Jovancic, J. Nedeljkovic, M. Radetic, *Carbohydr. Polym.* **2010**, *79*, 526.

[13] A. Morfesis, D. Fairhurst, at *NSTI Nanotechnology Conference and Trade Show. NSTI Nanotech* Anaheim, CA **May 8-12, 2005**.

[14] a) R. Brayner, R. Ferrari-Iliou, N. Brivois, S. Djediat, M. F. Benedetti, F. Fiévet, *Nano Lett.* **2006**, *6*, 866; b) K. M. Reddy, K. Feris, J. Bell, D. G. Wingett, C. Hanley, A. Punnoose, *Appl. Phys. Lett.* **2007**, *90*, 213902; c) C. Hanley, C. J. Layne, A. Punnose, K. M. Reddy, I. Coombs, A. Coombs, K. Feris, D. Wingett, *Nanotechnology* **2008**, *19*, 295103; d) Z. Huang, X. Zheng, D. Yan, G. Yin, X. Liao, Y. Kang, Y. Yao, D. Huang, B. Hao, *Langmuir* **2008**, *24*, 4140; e) N. Padmavathy, R. Vijayaraghavan, *Sci. Technol. Adv. Mater.* **2008**, *9*, 035004; f) C. Karunakaran, P. Gomathisankar, G. Manikandan, *Mater. Chem. Phys.* **2010**, *123*, 585.

[15] a) L. L. Zhang, Y. H. Jiang, Y. L. Ding, N. Daskalakis, L. Jeuken, M. Povey, A. J. O'Neill, D. W. York, *J. Nanopart. Res.* **2010**, *12*, 1625; b) M. Li, L. Z. Zhu, D. H. Lin, *Environ. Sci. Technol.* **2011**, *45*, 1977.

[16] a) S. Nair, A. Sasidharan, V. V. Divya Rani, D. Menon, S. Nair, K. Manzoor, S. Raina, *J. Mater. Sci. Mater. Med.* **2009**, *20*, 235; b) W. Song, J. Zhang, J. Guo, J. Zhang, F. Ding, L. Li, Z. Sun, *Toxicol. Lett.* **2010**, *199*, 389; c) B. De Berardis, G. Civitelli, M. Condello, P. Lista, R. Pozzi, G. Arancia, S. Meschini, *Toxicol. Appl. Pharm.* **2010**, *246*, 116.

[17] A. L. Incoronato, A. Conte, G. G. Buonocore, M. A. Del Nobile, *J. Dairy Sci.* **2011**, *94*, 1697.

[18] a) T. Yamashita, Y. Tanaka, N. Idota, K. Sato, K. Mawatari, T. Kitamori, *Biomaterials* **2011**, *32*, 2459; b) J. Yang, M. Yamato, T. Shimizu, H. Sekine, K. Ohashi, M. Kanzaki, T. Ohki, K. Nishida, T. Okano, *Biomaterials* **2007**, *28*, 5033; c) A. R. C. Duarte, J. F. Mano, R. L. Reis, *Acta Biomater.* **2011**, *7*, 526; d) M. E. Nash, W. M. Carrol, N. Nikoloskya, R. Yang, C. O'Connell, A. V. Gorelov, P. Docery, C. Liptrot, F. M. Lyng, A. Garcia, Y. A. Rochev, *ACS Appl. Mater. Interfaces* **2011**, *3*, 1980.

[19] L. K. Ista, G. P. Lopez, *J. Ind. Microbiol. Biotechnol.* **1998**, *20*, 121.

[20] a) J. F. Mano, *Adv. Eng. Mater.* **2008**, *10*, 515; b) M. A. Cole, N. H. Voelcker, H. Thissen, H. J. Griesser, *Biomaterials* **2009**, *30*, 1827; c) N. A. Peppas, J. Z. Hilt, A. Khademhosseini, R. Langer, *Adv. Mater.* **2006**, *18*, 1345.

[21] P. Schexnailder, G. Schmidt, *Colloid Polym. Sci.* **2009**, *287*, 1.
[22] C. R. van den Brom, I. Anac, R. F. Roskamp, M. Retsch, U. Jonas, B. Menges, J. A. Preece, *J. Mater. Chem.* **2010**, *20*, 4827.
[23] a) A. Agarwal, T. L. Weis, M. J. Schurr, N. G. Faith, C. J. Czuprynski, J. F. McAnulty, C. J. Murphy, N. L. Abbott, *Biomaterials* **2010**, *31*, 680; b) E. Korner, M. H. Aguirre, G. Fortunato, A. Ritter, J. Ruhe, D. Hegemann, *Plasma Process. Polym.* **2010**, *7*, 619; c) J. Gonzalez-Benito, G. Gonzalez-Gaitano, *Macromolecules* **2008**, *41*, 4777; d) R. F. Mulligan, A. A. Iliadis, P. Kofinas, *J. Appl. Polym. Sci.* **2003**, *89*, 1058.
[24] M. R. Bockstaller, R. A. Mickiewicz, E. L. Thomas, *Adv. Mater.* **2005**, *17*, 1331.
[25] M. Agrawal, S. Gupta, N. E. Zafeiropoulos, U. Oertel, R. Häßler, M. Stamm, *Macromol. Chem. Phys.* **2010**, *211*, 1925.
[26] J. Park, J. Joo, S. G. Kwon, Y. Jang, T. Hyeon, *Angew. Chem. Int. Ed.* **2007**, *46*, 4630.
[27] K. Yang, D. H. Lin, B. S. Xing, *Langmuir* **2009**, *25*, 3571.
[28] a) H.-M. Xiong, Y. Xu, Q.-G. Ren, Y.-Y. Xia, *J. Am. Chem. Soc.* **2008**, *130*, 7522; b) S. John, S. Marpu, J. Y. Li, M. Omary, Z. B. Hu, Y. Fujita, A. Neogi, *J. Nanosci. Nanotechnol.* **2010**, *10*, 1707; c) L. Irimpan, B. Krishnan, A. Deepthy, V. P. N. Nampoori, P. Radhakrishnan, *J. Phys. D Appl. Phys.* **2007**, *40*, 5670.
[29] L. Duque, R. Förch, *Plasma Process. Polym.* **2011**, *8*, 444.
[30] a) A. A. Tayel, W. F. El-Tras, S. Moussa, A. F. El-Baz, H. Mahrous, M. F. Salem, L. Brimer, *J. Food Saf.* **2011**, *31*, 211; b) K. R. Raghupathi, R. T. Koodali, A. C. Manna, *Langmuir* **2011**, *27*, 4020.
[31] a) J. T. Seil, T. J. Webster, *Acta Biomater.* **2011**, *7*, 2579; b) X. H. Li, Y. G. Xing, W. L. Li, Y. H. Jiang, Y. L. Ding, *Food Sci. Technol. Int.* **2010**, *16*, 0225; c)X. Li, Y. Xing, Y. Jiang, Y. Ding, W. Li, *Int. J. Food Sci. Technol.* **2009**, *44*, 2161.
[32] a) N. Jones, B. Ray, K. T. Ranjit, A. C. Manna, *FEMS Microbiol. Lett.* **2008**, *279*, 71; b) G. Applerot, A. Lipovsky, R. Dror, N. Perkas, Y. Nitzan, R. Lubart, A. Gedanken, *Adv. Funct. Mater.* **2009**, *19*, 842.
[33] a) J. Sawai, H. Igarashi, A. Hashimoto, T. Kokugan, M. Shimizu, *J. Chem. Eng. Jpn.* **1996**, *29*, 251; b) O. Yamamoto, M. Komatsu, J. Sawa, Z. E. Nakagawa, *J. Mater. Sci. Mater. Med.* **2004**, *15*, 847; c) L. Zhang, Y. Jiang, Y. Ding, M. Povey, D. York, *J. Nanopart. Res.* **2007**, *9*, 479.
[34] P. K. Stoimenov, R. L. Klinger, G. L. Marchin, K. J. Klabunde, *Langmuir* **2002**, *18*, 6679.
[35] J. Sawai, E. Kawada, F. Kanou, H. Igarashi, A. Hashimoto, T. Kokugan, M. Shimizu, *J. Chem. Eng. Jpn.* **1996**, *29*, 627.
[36] E. Ruoslahti, J. C. Reed, *Cell* **1994**, *77*, 477.
[37] A. Aulasevich, R. F. Roskamp, U. Jonas, B. Menges, J. Dostálek, W. Knoll, *Macromol. Rapid Commun.* **2009**, *30*, 872.
[38] a) C. Hanley, J. Layne, A. Punnoose, K. M. Reddy, I. Coombs, A. Coombs, K. Feris, D. Wingett, *Nanotechnology* **2008**, *19*, 295103; b) S. Ostrovsky, G. Kazimirsky, A. Gedanken, C. Brodie, *Nano Res* **2009**, *2*, 882; c) L. Taccola, V. Raffa, C. Riggio, O. Vittorio, M. C. Iorio, R. Vanacore, A. Pietrabissa, A. Cuschieri, *Int. J. Nanomed.* **2011**, *6*, 1129.
[39] a) A. Ben-Ze'ev, S. R. Farmer, S. Penman, *Cell* **1980**, *21*, 365; b) S. M. Frisch, H. Francis, *J. Cell Biol.* **1994**, *124*, 619; c) J. E. Meredith Jr., M. A. Schwartz, *Trends Cell Biol.* **1997**, *7*, 146.
[40] a) M. J. Richards, J. R. Edwards, D. H. Culver, R. P. Gaynes, *Infect. Control. Hosp. Epidemiol.* **2000**, *21*, 510; b) M. L. Kilgore, K. Ghosh, C. M. Beavers, D. Y. Wong, P. A. Hymel Jr., S. E. Brossette, *Med. Care* **2008**, *46*, 101; c) M. Kilgore, S. Brossette, *Am. J. Infect. Control* **2008**, *36*, 171.
[41] P. W. Beines, I. Klosterkamp, B. Menges, U. Jonas, W. Knoll, *Langmuir* **2007**, *23*, 2231.
[42] J. Ludbrook, *Cardiovasc. Res.* **1994**, *28*, 303.
[43] Y. Waseda, E. Matsubara, K. Shinoda, *X-Ray Diffraction Crystallography*, Springer-Verlag, Berlin, Heidelberg, **2011**.